

Predicting solar flares with machine learning: investigating solar cycle dependence

XIANTONG WANG,¹ YANG CHEN,² GABOR TOH,¹ WARD B. MANCHESTER,¹ TAMAS I. GOMBOSI,¹ ALFRED O. HERO,³
ZHENBANG JIAO,² HU SUN,² MENG JIN,^{4,5} AND YANG LIU⁶

¹*Department of Climate and Space Sciences and Engineering, University of Michigan
Ann Arbor, MI, USA*

²*Department of Statistics, University of Michigan
Ann Arbor, MI, USA*

³*Department of Electrical Engineering and Computer Science, University of Michigan
Ann Arbor, MI, USA*

⁴*Lockheed Martin Solar and Astrophysics Laboratory, Palo Alto, California, USA*

⁵*SETI Institute, Mountain View, CA 94043, USA*

⁶*Hansen Experimental Physics Laboratory, Stanford University, Stanford, CA 94305, USA*

ABSTRACT

A deep learning network, Long-Short Term Memory (LSTM) network, is used in this work to predict whether the maximum flare class an active region (AR) will produce in the next 24 hours is class Γ . We considered Γ are $\geq M$, $\geq C$ and any flare class. The essence of using LSTM, which is a recurrent neural network, is its capability to capture temporal information of the data samples. The input features are time sequences of 20 magnetic parameters from SHARPs - Space-weather HMI Active Region Patches. We analyzed active regions from June 2010 to Dec 2018, using the Geostationary Operational Environmental Satellite (GOES) X-ray flare catalogs and label the data samples with identified ARs in the GOES X-ray flare catalogs. Our results (i) shows consistent skill scores with recently published results using LSTMs and better than the previous work using single time input (eg. DeFN) (ii) The skill scores from the model show essential differences when different years of data was chosen for training and testing.

Keywords: magnetic fields — methods: statistical — Sun: activity — Sun: chromosphere — Sun: flare

1. INTRODUCTION

Solar flares are large electromagnetic radiation eruptions from the Sun with lasting time varies from minutes to hours. Meanwhile, massive amount of energy is released during the process. The influence of small flares is limited while the others can be tremendous and violent. Strong flares are often accompanied with coronal mass ejections (CMEs) which can cause more substantial influences on the Earth environment. Therefore, it is significant to make efforts on predicting solar flares especially larger ones. However, during solar cycle 24, there were more than 2000 M flares with only less than 180 X flares, the rareness of the extreme events and the complexity of the flares make solar flare time and intensity predictions a challenging task.

Although the triggering mechanism of solar flares and the determiner of the solar flare strength are far from well understood, it is shown by multiple studies that solar flares are highly related to the sudden release of the magnetic free energy by magnetic reconnection in the coronal field. Since the photospheric magnetic field drives the coronal field, it's possible that the evolution patterns of the photospheric magnetic field features are indicators of the triggering process of flares and CMEs. Those features include the size of the active regions (AR), the integrated magnetic flux, the integrated current helicity, the magnetic field gradient measurements, the shear angle of the magnetic field structure and so on. The Helioseismic and Magnetic Imager (HMI) on the Solar Dynamics Observatory (SDO) satellite

launched a decade ago has tremendous amount of photospheric magnetic field observations from 2010. The Space-weather HMI Active Region Patches, or SHARPs (Bobra et al. 2014) contains those features pre-calculated based on the AR magnetic field observations, which is the data we will investigate on.

Machine learning, as a subfield of the artificial intelligence technology, utilizes the past data as a "learning context" for the computer program and let it make predictions on the data which never be seen before. Machine learning algorithms are started being applied to predict solar activities during the past decades. At first, the line-of-sight (LOS) component of the photospheric magnetic field measured by the by the Michelson Doppler Imager (MDI) instrument aboard the SOHO (Solar & Heliospheric Observatory) spacecraft was used by several groups to forecast solar flares using machine learning algorithms (Ahmed et al. (2013), Huang et al. (2018), Song et al. (2009), Yu et al. (2009), Yuan et al. (2010)). Support vector machine (SVM) algorithm was used by Boucheron et al. (2015) for classification task on time series of MDI data from 2000 to 2010. LOS magnetic field component doesn't include all the magnetic field information, certain studies are conducted after the vector magnetic field data was available. Bobra & Couvidat (2015) used the SVM trained with SHARPs parameters for active region classification tasks. Nishizuka et al. (2018) built a residual deep neural network using not only the parameterized photospheric magnetograms but also using chromospheric images. Jonas et al. (2018) used observations from photosphere, chromosphere, transition region, and corona as input of the machine learning algorithm, which has a comparable result with the works done by Bobra & Couvidat (2015) and Nishizuka et al. (2018). The machine learning algorithms in the studies mentioned so far are not fully utilizing the time dependent input. Among variant kinds of machine learning algorithms, recurrent neural networks (RNNs) are considered to be able to analyze the time series input. Long-short term memory networks (LSTMs) (Hochreiter & Schmidhuber 1997; Gers et al. 1999) as one of the RNNs can learn the order dependence between samples in a sequence have succeeded in many sequence classification and prediction tasks, including speech recognition, time-series forecasting, handwriting recognition and so on (Hastie et al. 2005; Graves et al. 2013). Liu et al. (2019) firstly used LSTMs on SHARPs parameters, which achieved better performance for predicting solar flares compared to previous works.

In this paper, we applied the LSTM algorithm on the SHARPs parameters from SDO/HMI vector magnetic field to predict the maximum solar flare class will happen in an active region after 24 hours. The inputs are 48 hours time series of SHARPs parameters with 12 minutes cadence. The observations of ARs are time sequences hence LSTMs are suitable for this kind of input. Not only our results shows consistent results with recently published work by Liu et al. (2019) which also using LSTM algorithm, but also we found that by using different years of ARs in training and testing set, the skill scores vary substantially, which indicates that data samples should be carefully chosen when we make evaluations of models.

The rest of this paper is organized as follows. Section 2 describes how we collected data and built the training and testing sets. Section 3 describes the LSTM architecture we are using in the paper. Section 4 illustrates the metrics used to evaluate the model performance, Section 5 shows the results of this work and comparisons with previous models, the results of model's solar cycle dependence are also presented in this section. Section 6 includes the conclusion.

2. DETAILS OF THE DATA PREPARATION

2.1. Constructing dataset

We use SHARP summary parameters as the input data of the prediction model. SHARPs - Space-weather HMI Active Region Patches is a data product from the *Helioseismic and Magnetic Imager* (HMI) onboard the *Solar Dynamics Observatory* (SDO) (Bobra et al. 2014). The summary parameters are calculated based on the *HMI Active Region Patches* (HARPs) which are rectangular boxes on the active regions moving with the solar rotation. Twenty key parameters are used in this work and are described in Table 2. The SHARP summary parameters are downloaded based on active regions from [Joint Science Operations Center \(jsoc.stanford.edu\)](http://jsoc.stanford.edu) and data from 2011 to 2018 is collected. The solar flare events are from the NOAA Geostationary Operational Environmental Satellites (GOES) flare list (Garcia 1994). In GOES flare list, flare events are listed with class, start, end, and peak intensity time of each event. The peak time of the flare events are assigned as the "event time" when constructing the data samples. The number of active regions and flare events in different years are summarized in the Table 1. We noticed that the number of C flares outnumbers the B flares and the reason could be many B flares are missed due to the active background.

The time sequences as the input of the model are extracted from the SHARP summary parameters. The criterion of selecting time sequences are described as follows:

Table 1. The number of active regions and different classes of flares in each year, notice that a lot of A and B flares are missing.

Year	ARs	A	B	C	M	X
2011	168	1	665	1002	106	9
2012	168	0	475	1115	124	7
2013	183	0	469	1197	97	12
2014	194	0	184	1627	194	16
2015	143	0	446	1274	128	2
2016	109	0	757	294	15	0
2017	52	0	620	229	37	4
2018	21	5	255	12	0	0

1. In order to avoid projection effects, the longitude of the HARP region center is within the range of $\pm 68^\circ$ from the central meridian.
2. The percentage of the missing frame in a time sequence is less than 5%
3. The time difference between the starting time of two sequences is 1 hour

The target value (or label) of each sequence is the maximum flare class of this certain active region in the next 24h after the end time of this sequence. The NOAA active region number is used to match the HARP and ARs in the GOES flare list. The GOES flares are identified strictly with NOAA ARs, while we notice that a single AR is split between HARPs or a HARP contains multiple ARs. Our examination shows that 20% of HARP have this mismatching issue which may lead to a potential error when we assign targets to sequences. In the future work, we will address this problem by splitting the HARP regions to multiple ARs or combine multiple HARP regions into one and recalculate the SHARP summary parameters.

Because the features have different scales and units, the original data samples are normalized before input into the machine learning model: let z_i^n denote the normalized value of the i th feature in n th data sample, then

$$z_i^n = \frac{v_i^n - \mu_i}{\sigma_i} \quad (1)$$

where v_i^n is the original value of the i th feature in n th data sample and μ_i, σ_i are the mean and standard deviation of the i th feature calculated from the entire dataset.

2.2. Training/Testing splitting

In order to assess the performance of the machine learning algorithms properly, we need to split the samples (time sequences of SHARP summary parameters and corresponding maximum flare classes) into a training set and a testing set. The training set is used for training the machine learning model while the testing set is for assessing the prediction ability of the model. In the training process, the model should learn from the input data and adjusts its parameters to fit the ground truth. Both variable selection and parameter estimation are included in this process. The samples in the testing set should be totally separated from the training set, otherwise there will be an artificial gain of performance since the information in the training set is leaked to the test set. Hence separating the samples based on active regions is necessary to guarantee that sequences from one active region will not occur in both training and testing sets simultaneously. All the training/testing splitting in this paper are conducted based on active regions.

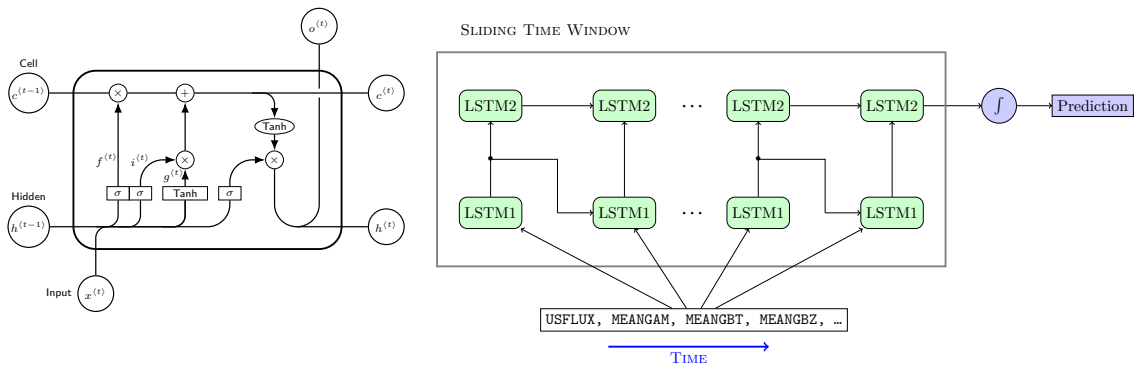
3. ARCHITECTURE OF SEQUENCE MODEL

Recurrent Neural Network (RNN) is a category of neural networks which can make use of sequential information. This architecture is naturally used in solar flare prediction since the active regions evolve with time and the occurrence

Table 2. List of SHARP parameters and brief descriptions

Parameter	Description
USFLUX	Total unsigned flux in Maxwells
MEANGAM	Mean inclination angle, gamma, in degrees
MEANGBT	Mean value of the total field gradient, in Gauss/Mm
MEANGBZ	Mean value of the vertical field gradient, in Gauss/Mm
MEANGBH	Mean value of the horizontal field gradient, in Gauss/Mm
MEANJZD	Mean vertical current density, in mA/m^2
TOTUSJZ	Total unsigned vertical current, in Amperes
MEANALP	Total twist parameter, alpha, in $1/\text{Mm}$
MEANJZH	Mean current helicity in G^2/m
TOTUSJH	Total unsigned current helicity in G^2/m
ABSNJZH	Absolute value of the net current helicity in G^2/m
SAVNCPP	Sum of the Absolute Value of the Net Currents Per Polarity in Amperes
MEANPOT	Mean photospheric excess magnetic energy density in ergs per cubic centimeter
TOTPOT	Total photospheric magnetic energy density in ergs per cubic centimeter
MEANSHR	Mean shear angle (measured using B_{total}) in degrees
SHRGT45	Percentage of pixels with a mean shear angle greater than 45 degrees in percent
SIZE	Projected area of patch on image in micro-hemisphere
SIZE_ACR	Projected area of active pixels on image in micro-hemisphere
NACR	Number of active pixels in patch
NPIX	Number of pixels within the patch

of the solar flares is relate to the time-dependent patterns of active regions. RNNs are called recurrent because they perform the same task for every input from the sequence, with the output being depended on the previous computations. Among varies of RNN structures, Long Short Term Memory (LSTM) is one of the most commonly used type of RNNs. As a special kind of RNN, LSTM networks (LSTMs) are explicitly designed to avoid the long-term dependency problem which is a major shortcoming for primitive RNNs. The key to LSTMs is a new variable in the network called cell state, it is passed through the whole chain with only minor linear interactions which allows the information at a much earlier time of the input has effects longer time later.

**Figure 1.** The detailed structure of the LSTM cell (left) and the LSTM network (right)

The structure of the LSTM unit and the LSTM network used in this work is shown in Figure 1. The left panel of the Figure 1 is the detail of a single LSTM unit, each unit takes a input vector $x^{<t>}$ which are the input features

at a certain time point, the hidden state $h^{<t-1>}$ and the cell state $c^{<t-1>}$ are from the previous LSTM unit. The right panel is the structure of the two-layer LSTM network be used in this work. Multilayer LSTMs are widely used recently in The LSTM units in the second layer are the same as the first layer, while the input vectors are the output $o^{<t>}$ from the first layer LSTM units. The relationship between the unit output and input is shown in equation 3. The σ is the sigmoid function 2 which introduces the non-linearity into the architecture:

$$\sigma(x) = \frac{1}{1 + e^{-x}} \quad (2)$$

$x^{<t>} \in \mathbb{R}^d$ is the input vector to the LSTM unit, d is the number of features. $i^{<t>} \in \mathbb{R}^h, f^{<t>} \in \mathbb{R}^h, o^{<t>} \in \mathbb{R}^h$ are the input gate's, forget gate's and output gate's activation vectors, $g^{<t>} \in \mathbb{R}^h$ is also a activation vector from the tanh function. h is the hidden dimension of the LSTM unit which is a hyperparameter in the model which reflects the complexity. $c^{<t>} \in \mathbb{R}^h$ is the cell state vector and there is only linear relationship between the output and input cell states in a single LSTM unit. $W_{i-} \in \mathbb{R}^{h \times d}$ are the weight matrices applied on the input vectors and $W_{h-} \in \mathbb{R}^{h \times h}$ are the weight matrices applied on the gate activation vectors. $b \in \mathbb{R}^h$ in the equation are the bias vectors. The weight matrices and bias vectors are trainable parameters which will be updated during the optimization process.

$$i^{<t>} = \sigma(W_{ii}x^{<t>} + b_{ii} + W_{hi}h^{<t-1>} + b_{hi}) \quad (3a)$$

$$f^{<t>} = \sigma(W_{if}x^{<t>} + b_{if} + W_{hf}h^{<t-1>} + b_{hf}) \quad (3b)$$

$$g^{<t>} = \tanh(W_{ig}x^{<t>} + b_{ig} + W_{hg}h^{<t-1>} + b_{hg}) \quad (3c)$$

$$o^{<t>} = \sigma(W_{io}x^{<t>} + b_{io} + W_{ho}h^{<t-1>} + b_{ho}) \quad (3d)$$

$$c^{<t>} = f^{<t>} * c^{<t-1>} + i^{<t>} * g^{<t>} \quad (3e)$$

$$h^{<t>} = o^{<t>} * \tanh(c^{<t>}) \quad (3f)$$

The "training" in the machine learning is essentially an optimization process for a objective function, also known as loss function. The loss function measures the difference between model's prediction and the ground truth. An optimization algorithm is used to minimize the loss function so that the trainable parameters in the model can "encode" some knowledge from the data samples. "Binary Cross Entropy" is used as the loss function for binary classification problems. However, this loss function can fail if one category of samples is dominating the entire dataset. Because constantly predicting the dominant category in the testing set can result in a small value of the loss function while the model has no predictability in this case. Solar flares are extremely rare events so that the dataset we are using is highly unbalanced. To solve this issue, we used "Binary Cross Entropy with Logits Loss" in this work which is described as:

$$L = \frac{1}{N} \sum_n -[p_c y_n \log \sigma(\hat{y}_n) + (1 - y_n) \log(1 - \sigma(\hat{y}_n))] \quad (4)$$

N is the number of samples in the testing set, y_n is the target value and \hat{y}_n is the model output. p_c and the sigmoid function are the differences of this loss function and the normal binary cross entropy loss. Sigmoid function improves the numerical stability in the optimization process. p_c is the ratio of negative and positive samples. In this work, this value is calculated from the training set.

4. MODEL EVALUATION

The HSS (Heidke Skill Score), TSS (True Skill Score), ACC (Accuracy), FAR (False Alarm Rate), Recall (also known as Probability of Detection, POD) and Precision are used to evaluate the model's predictability. These skill

scores are defined as follows, in which TN, TP, FN, FP referring to True Negative, True Positive, False Negative and False Positive.

$$\text{HSS} = \frac{2(\text{TP} \cdot \text{TN} - \text{FP} \cdot \text{FN})}{(\text{TP} + \text{FN})(\text{FN} + \text{TN}) + (\text{TP} + \text{FP})(\text{FP} + \text{TN})} \quad (5a)$$

$$\text{TSS} = \frac{\text{TP}}{\text{TP} + \text{FN}} - \frac{\text{FP}}{\text{FP} + \text{TN}} \quad (5b)$$

$$\text{ACC} = \frac{\text{TP} + \text{TN}}{\text{TP} + \text{FP} + \text{FN} + \text{TN}} \quad (5c)$$

$$\text{FAR} = \frac{\text{FP}}{\text{FP} + \text{TN}} \quad (5d)$$

$$\text{Recall} = \text{POD} = \frac{\text{TP}}{\text{TP} + \text{FN}} \quad (5e)$$

$$\text{Precision} = \frac{\text{TP}}{\text{TP} + \text{FP}} \quad (5f)$$

$$(5g)$$

5. RESULTS

5.1. Training Process

The LSTM network is implemented in Python with PyTorch package. PyTorch is originally a tensor calculation package for GPU and the auto gradient feature makes it suitable for machine learning tasks. A minibatch strategy is used for faster convergence during back-propagation. The optimizer used is Adam. The learning rate is set to 0.001, β_1 and β_2 are set to 0.9 and 0.999. The batch size is 1000. The model is trained for multiple epochs on the training set. In each epoch, the model goes through the training samples once. We examined the loss function history after each epoch and the loss function will not drop further after 2 or 3 epochs. To provide a fair comparison, the model is trained for 6 epochs to generate the results presented in Table 3, Figure 3 and Figure 4. Because of the randomness such as the order of loading training samples, the parameter initialization exists in the training process. We set up 20 independent runs with different random seeds and the mean values of the skill scores are collected in the Table3.

5.2. Skill scores for solar flare prediction

The mean value of skill scores for 20 runs are collected in the Table 3 and results produced by previous models are also listed. From Table 3, the skill scores for predicting $\geq C$ flares is larger than predicting $\geq M$ flares in all different models. However, the skill scores for predicting any flares ($> Q$) is smaller than predicting $\geq C$ flares. The reason to the smaller skill scores for predicting any flares is the missing positive samples in the dataset. The number of flares in different classes should obey roughly a power-law distribution (see Figure 8) thus a large number of class B flares are missing in the GOES flare records (see Figure 2). The EUV emission of lot of B flares are smaller than the background emission level which causes those B flares unrecorded. Therefore, we are training and testing the model with wrong data samples for prediction any class of flares hence lots of TPs in the testing results are classified as FPs.

5.3. Comparison with previous results

In this subsection, we will compare the results between our model and previously published works. In the past decade, there are several works using machine learning based models to predict solar flares, those models including MLP (Multilayer perceptrons) (Florios et al. 2018), SVM (Support Vector Machine) (Qahwaji & Colak 2007; Yuan et al. 2010; Bobra & Couvidat 2015; Boucheron et al. 2015; Muranushi et al. 2015; Florios et al. 2018), RF (Random Forest) (Barnes et al. 2016; Liu et al. 2017; Florios et al. 2018), DeFN (Deep Flare Net) (Nishizuka et al. 2018) and a recently published work which also used LSTM network. The prediction can be finally reduced to a binary classification task: according to the given input, will this AR produce a flare larger than a certain class or not in the next 24 hours. The model will generate a prediction score in the last layer in the network and if this score is larger than a certain threshold, then this AR will produce a flare within T hours and otherwise, this AR will not produce a flare in the next 24 hours. In our work, the last layer is a sigmoid function and the output from a sigmoid function is either close to 0 or 1, so the threshold for binary classification is set to be 0.5.

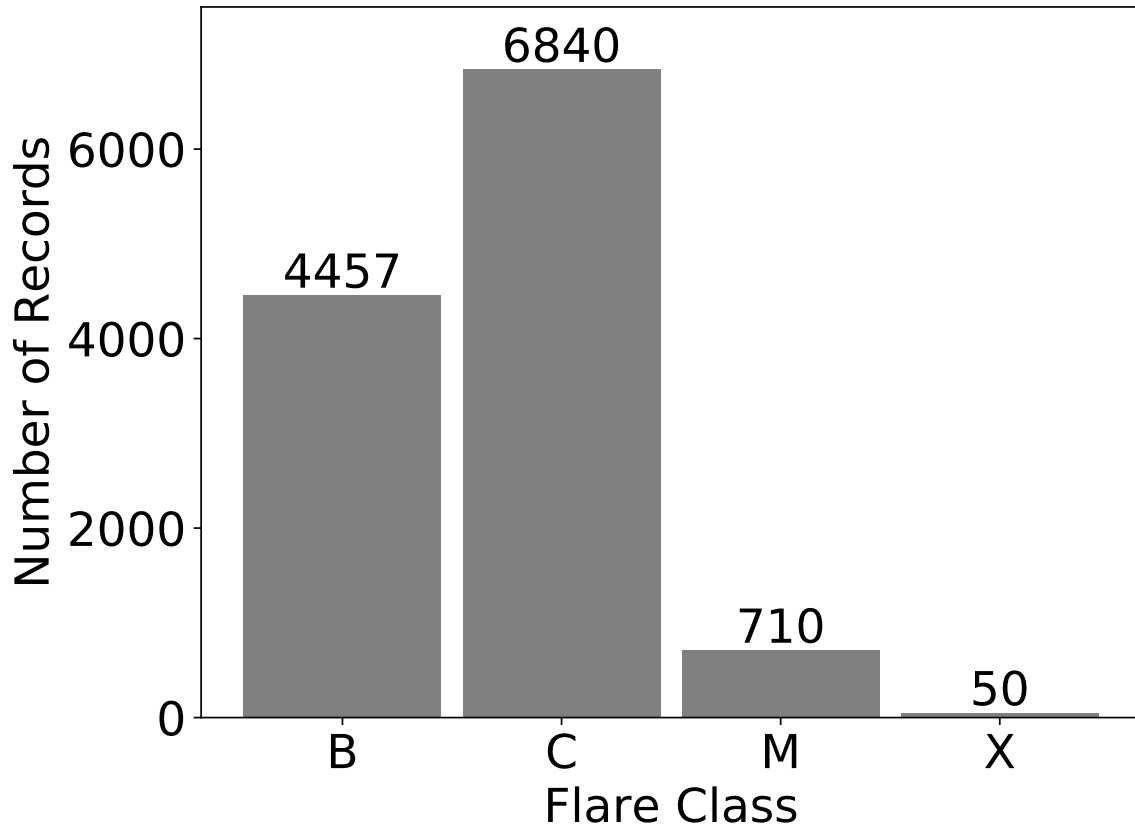


Figure 2. The distribution of number of flares for classes *B, C, M, X*, the number of *B* flares is much less than the number of *C* flares.

The values of evaluations metrics for different models are shown in Table 3. Even though the input and the testing samples may different in those works using MLP, SVM, DeFN and RF models, the results still represent the best performance of those models can achieve on the solar flare prediction task. The results of LSTM model outperform the previous models substantially, which indicates that taking time series data into account can make a difference in solar flare forecasting. As discussed in subsection 5.4, we must have relatively similar testing set to evaluate the model using skill scores since certain bias exists in different train/test splitting, especially chronological. The testing set in LSTM-2015 and DeFN are all use flare events in 2015 for testing, and for LSTM-Liu and LSTM-15_18 are all using events from 2015 to 2018 for testing. Among those evaluation metrics, **1.** Accuracy (ACC) is the most straightforward one since the dataset is highly biased (flare events are rare so the majority samples in the testing set are negative), predicting those negative samples correctly leads to a high accuracy however not much predictability for strong flare events are illustrated. **2.** Precision and Recall are usually analyzed together as a pair which reflects the model's ability of making positive predictions: Precision means among the predicted positive samples, what's the percentage of correctly predicted samples. Recall reflects the percentage of correctly predicted positive samples in the testing set. So that Precision reflects more predictability since it's evaluate based on the positive predicted samples from the model. From the Table 3, our model get the Precision score within the same range with Liu et al. (2019), and is better than the previous works listed. **3.** HSS and TSS are another pair which is often been discussed together. They are considered as better metrics for evaluating model predictability in binary classification tasks. However, TSS benefits from the large number of correctly predicted negative samples (TN) so that it's much higher than the HSS in all tests. HSS lessens the importance of TN but is more sensitive to the number of positive samples in the testing set: the value of HSS can be artificially improved if there are more positive samples in the testing set. Our model gives better HSS than previous models without using time sequences and also has the similar performance with the recent published result using LSTM, which validates the correctness of this work. **4.** False Alarm Rates (FAR) produced by the model are also presented in the Table 3. Different from other skill scores, lower FAR indicates the model producing less false

Table 3. Comparison of skill scores for different models, lines with * are results from this work. LSTM-2015 has the same time range with the DeFN while LSTM-15_18 has the same time range with LSTM-Liu.

Metric	Model	$\geq M$ class	$\geq C$ class	Any Class	
Recall	MLP	0.812	0.637	-	
	SVM	0.692	0.746	-	
	DeFN	0.891	0.761	-	
	RF	0.850	0.727	-	
	LSTM-Liu	0.881	0.762	-	
	*	LSTM-2015	0.685	0.643	0.625
*	LSTM-15_18	0.730	0.621	0.530	
Precision	MLP	0.143	0.451	-	
	SVM	0.106	0.497	-	
	DeFN	0.173	0.497	-	
	RF	0.252	0.532	-	
	LSTM-Liu	0.222	0.544	-	
	*	LSTM-2015	0.311	0.677	0.670
*	LSTM-15_18	0.282	0.635	0.702	
ACC	MLP	0.855	0.778	-	
	SVM	0.824	0.803	-	
	DeFN	0.872	0.801	-	
	RF	0.924	0.822	-	
	LSTM-Liu	0.909	0.829	-	
	*	LSTM-2015	0.929	0.858	0.814
*	LSTM-15_18	0.945	0.883	0.800	
HSS	MLP	0.204	0.389	-	
	SVM	0.141	0.472	-	
	DeFN	0.253	0.476	-	
	RF	0.361	0.502	-	
	LSTM-Liu	0.347	0.539	-	
	*	LSTM-2015	0.394	0.567	0.519
*	LSTM-15_18	0.382	0.557	0.473	
TSS	MLP	0.669	0.449	-	
	SVM	0.520	0.562	-	
	DeFN	0.763	0.572	-	
	RF	0.776	0.572	-	
	LSTM-Liu	0.790	0.607	-	
	*	LSTM-2015	0.623	0.559	0.509
*	LSTM-15_18	0.681	0.553	0.439	
FAR	*	LSTM-2015	0.062	0.084	0.116
	*	LSTM-15_18	0.049	0.068	0.092

alarms. The FAR for predicting $\geq C$ and $\geq M$ flares are all less than 0.1 which means that more than 90% negative predictions from the model are correct. The details of two LSTM models are different but get similar results according to Table 3 which indicates the information contained in the SHARP parameters is limiting the skill scores.

5.4. Choosing different testing years

As described before in section 2.2, it is important to make the training and testing samples totally separated. However, does choosing different years of flares for testing can have different skill scores is still unclear since the previous works all used data before 2015 for training and after 2015 for testing. In this subsection, we conducted the training-testing process on different combinations of training and testing years. In Figure 3, we present the box plots of skill scores for testing year from 2011 to 2015. If one year is selected for testing, other four years left from 2011 to 2015 are used for training. For 20 independent runs for predicting $\geq C$ and $\geq M$ flares, training on 2011 to 2014 and testing on 2015 gives the best HSS and FAR. Testing on 2015 doesn't give the best TSS for predicting $\geq M$ flares while for predicting $\geq C$ flares, it has the highest TSS. Since Recall and FAR are directly related to how precisely the model making positive predictions, by comparing the Recall and FAR on different years, the model is quite "conserve" on making predictions on year 2015 data. The stronger tendency of the model to make negative predictions will achieve a better FAR because less FPs are generated, meanwhile it will also bring down the Recall because the TPs are also reduced. Since the neural network structures and hyper-parameters are the same for all 5 tests, from Figure 3, evaluating the model performance on different years will introduce visible bias to the result.

To explain the model's tendency to make more negative predictions on year 2015, two linear regression models as baseline are used. These two baseline models take the training and testing samples exactly the same with previous LSTM model. The time sequences of SHARP parameters are reshaped to one-dimensional vectors as the input of the first linear regression model "Linear Regression A". For the second linear regression model "Linear Regression B", the mean values of the time sequences are taken as input. Twenty independent runs are conducted and the mean values of the skill scores from the LSTM model and two baseline models are shown in Figure 4. The difference between the LSTM model and the Linear Regression A is the non-linearity introduced by the LSTM network. The Linear Regression B eliminates the time sequence information and only inputs the average level of activity into the model. From Figure 4: **1.** For predicting $\geq M$ flares, the LSTM gives higher HSS than the linear regression models. For predicting $\geq C$ flares, the LSTM model has similar HSS with the Linear Regression A model which is still better than the Linear Regression B. This illustrates the importance of the time sequence information. **2.** The linear regression models give larger Recall and FAR according to Figure 4. So that the LSTM model has less tendency to make positive predictions which results in better HSS. The optimal case is the model produces high Recall while also keep a low FAR which is not the case for LSTM model. This is the reason why LSTM cannot provide a high TSS compare to Linear Regression models. **3.** All three models give the lowest FAR when testing on year 2015 and the results on other four years share the similar trend. This indicates that the reason for LSTM producing low FAR is related to the mean values of the SHARP parameters. In conclusion, the LSTM model produces more reliable positive predictions than the simple linear regression models although it will miss some positive events. The model gives different results when testing/training on different years of data which needs to be investigated furthermore.

5.5. Training/Testing on different solar cycle periods

According to subsection 5.4, training and testing on different years will give very different results. From Hoeksema et al. (2018), although the data processing techniques were modified in January, 2015, those changes will not have major effects on the data products used in this work. To investigate if there are any intrinsic differences of the active regions from each years, we will first do the training and testing separately on each year. Notice that the number of active regions and flares is very small from year 2016 to 2018, those three years will be grouped together. Four skill scores will be collected to evaluate the model performance: HSS, TSS, Recall and FAR. The process for selecting data samples is:

1. For active regions in each year, randomly select 25% for testing and rest of them for training,
2. Extract 48h time series of SHARP parameters for training and testing from active regions selected in step 1, the labels of the time series are the maximum flare class in the next 24 hours from the GOES flare record,
3. Randomly drop negative samples in the training and testing sets to fix the ratio of positive samples and negative samples to be 0.05 (for predicting $\geq M$ flares) and 0.3 (for predicting $\geq C$ flares).

Notice that in step 3, we fix the ratio of positive samples and negative samples to make the HSS directly comparable between different years. Since the dropping is done randomly for multiple times, each dataset is different from others.

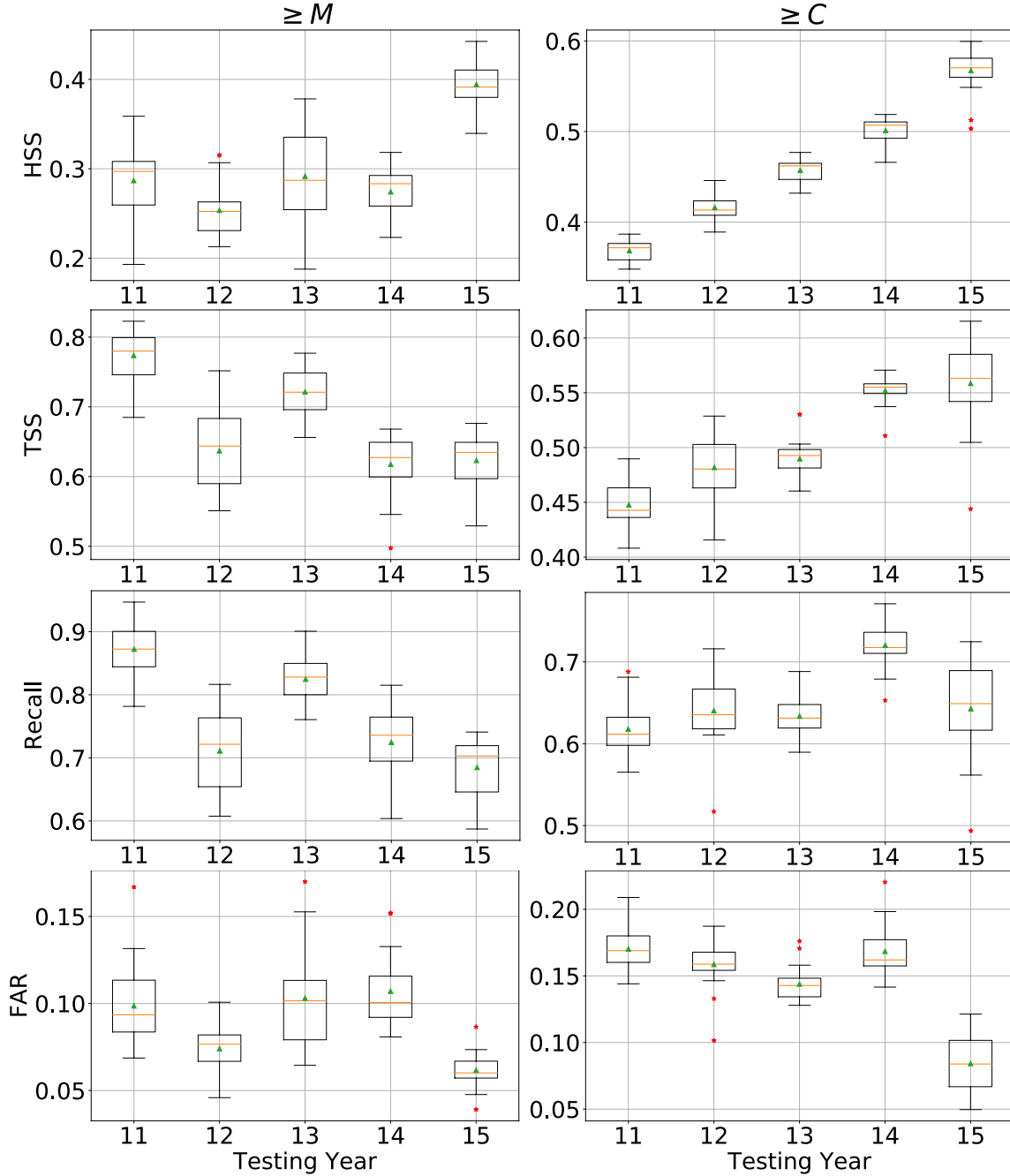


Figure 3. The box plots of 4 skill scores on different training and testing pairs. The positive flare class from left column to the right column is $\geq M$ and $\geq C$. Notice that smaller FAR means better performance. The yellow line is the median and the green triangle is the mean. The lower and upper bound of the box are the quartiles while the red stars are the data points outside the range of median $\pm 2.698\sigma$. The mean value and median are calculated including the outliers.

The skill scores are the mean values of the model outputs from 3 to 10 epochs. This could reflect the general performance of the model on these datasets without intentionally picking the best results for each dataset.

The boxplots of skill scores for predicting $\geq C$ flares are shown in Figure 5. Each box contains 100 data points from randomly selecting active regions for training/testing and dropping negative samples in the datasets. Because there are less active regions and flare events from year 2016 to 2018 according to Table 1, the skills scores are less centered and the number of outliers is larger than results from other years. From the boxplots, training and testing on the data after 2015 has better skill scores than other years. The FAR has the most substantial difference for datasets after and

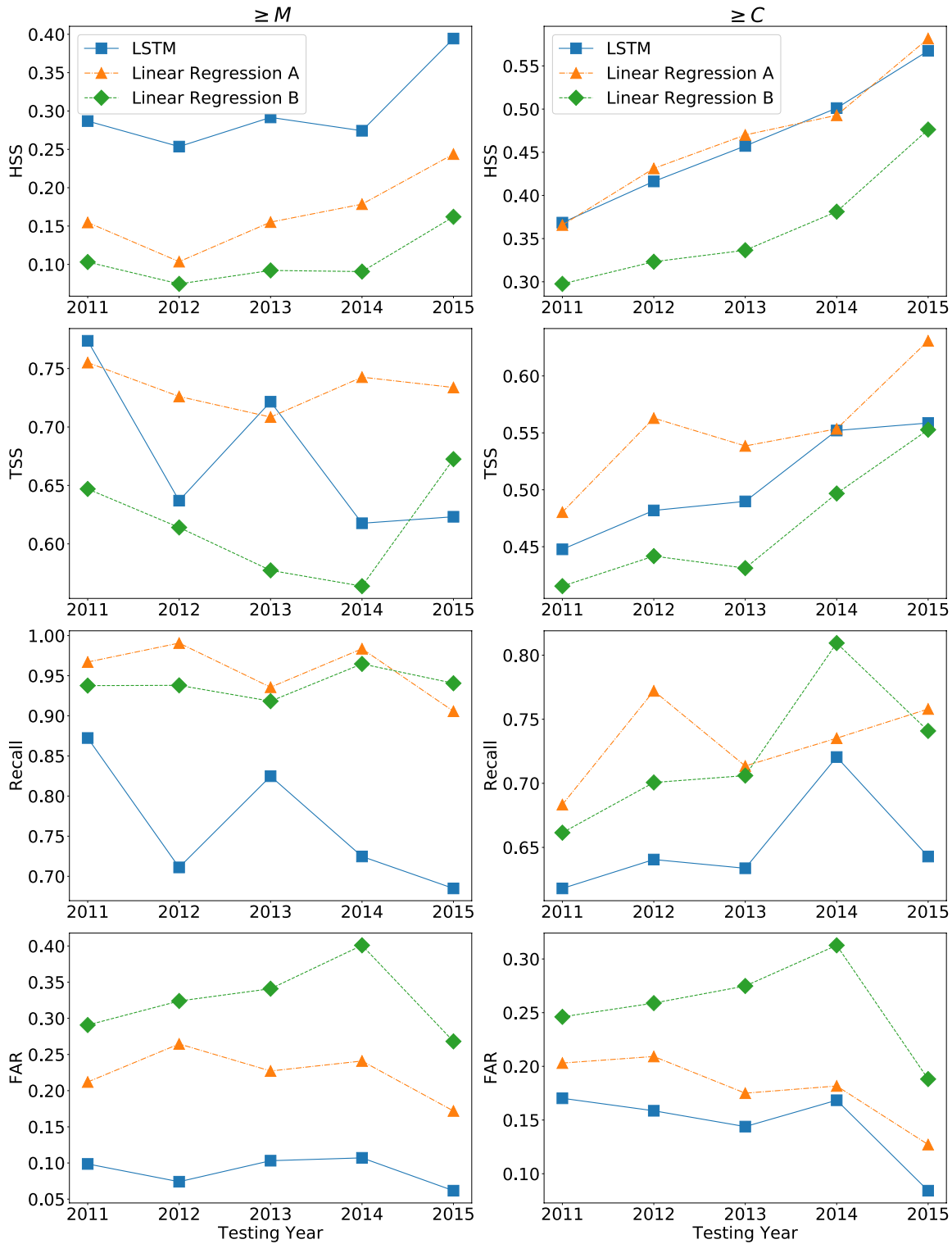


Figure 4. The comparison between LSTM model and two baseline linear regression models. Four skill scores are presented. Left column is the prediction for $\geq M$ flare and right column is for $\geq C$ flares. The Linear Regression A takes the whole time sequence as input (same as LSTM) and the Linear Regression B takes the mean value of the time sequence for each SHARP parameter.

before 2015 which is also the major reason to the better HSS and TSS since the recall don't vary much. We are not

showing results for predicting $\geq M$ flares on each year separately because the $\geq M$ flares are even more rare in each year and there is not much statistical pattern in the results.

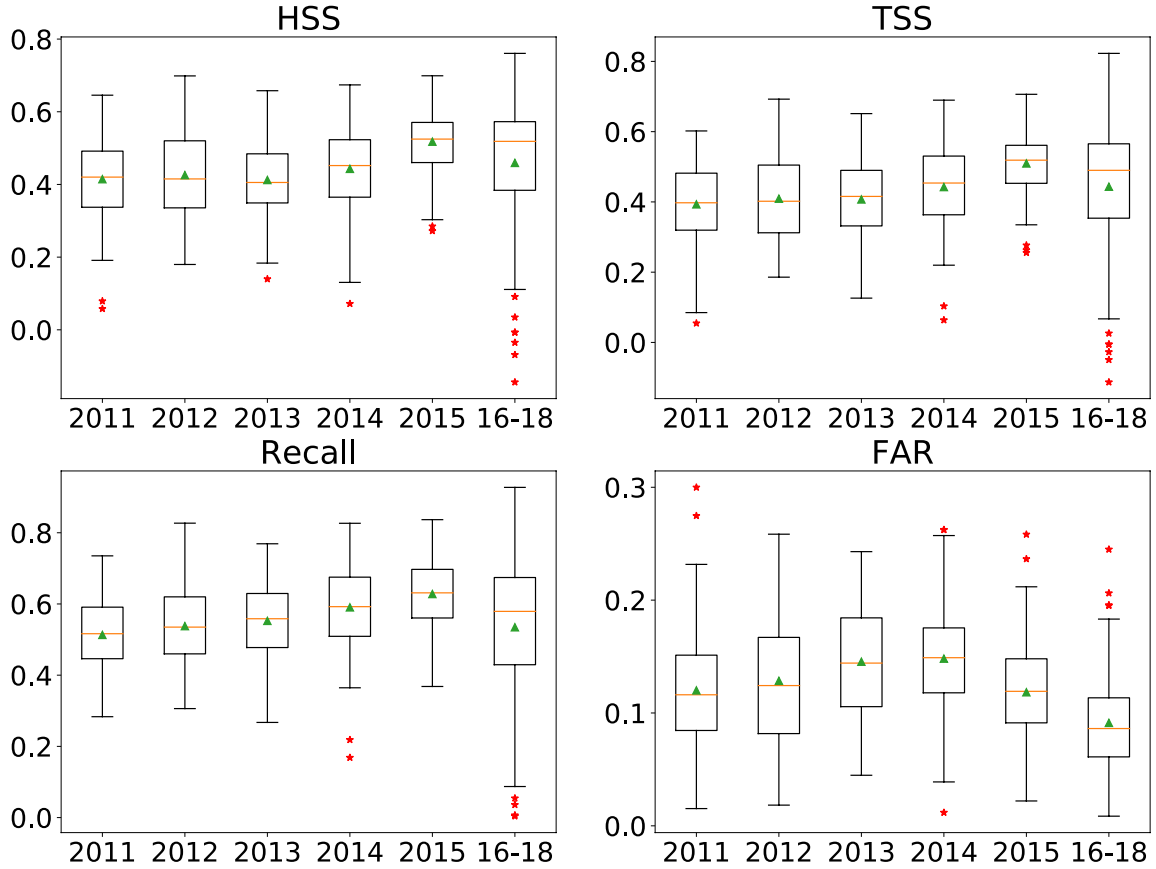


Figure 5. The box plots of skill scores for predicting $\geq C$ flares on different years from 2011 to 2018. The symbols in the figures are the same with previous boxplots.

From results shown in Figure 5, the prediction model has different performance on two groups of years separated by the start of year 2015. Furthermore, we will conduct the training/testing process on these two groups of years and the data selecting strategy is the same as what we did for training/testing on each year. The skill scores for predicting $\geq C$ flares are show in Figure 6 and Figure 7 shows the skill scores for predicting $\geq M$ flares. For predicting $\geq C$ flares, the boxes of HSS and TSS are more separated than skill scores for each year in Figure 5. The boxplots of Recall for those two datasets are overlapped with each other while the boxplots of FAR are well separated. Which indicates that for capturing $\geq C$ flares in the testing set, the model has similar performance when trained on the data samples from two phases in a solar cycle. However, the model will be produced much less false alarms if it is trained on data samples from the declining phase in a solar cycle. For predicting $\geq M$ flares, according to Figure 7, the difference of skill scores is less obvious. In general, the result of year 2015-2018 shows larger variance because there are less $\geq M$ flares in this time range. The boxplots of HSS, TSS and Recall are overlapped to a large extent except the model gives a higher FAR when trained/tested on year 2015-2018. The reason to the different skill scores for predicting $\geq C$ and $\geq M$ flares could be the different flare intensity distribution in two phases in a solar cycle. If the C flares and M flares are distributed more continuously, it's more difficult for the model to identify between the C and M flares which leads to lower skill scores. Figure 8 shows the flare events number distribution in log-log scale for C and M flares intensity in two groups of years. The straight lines in the histogram in log-log scales indicates the flare intensity obeys with the power law distribution. However, the slope of two lines are very close to each other which shows that there is no obvious difference in the flare intensity distribution of two phases of a solar cycle. The difference of the skill scores in Figure 6 and 7 is not because of the different flare intensity distributions.

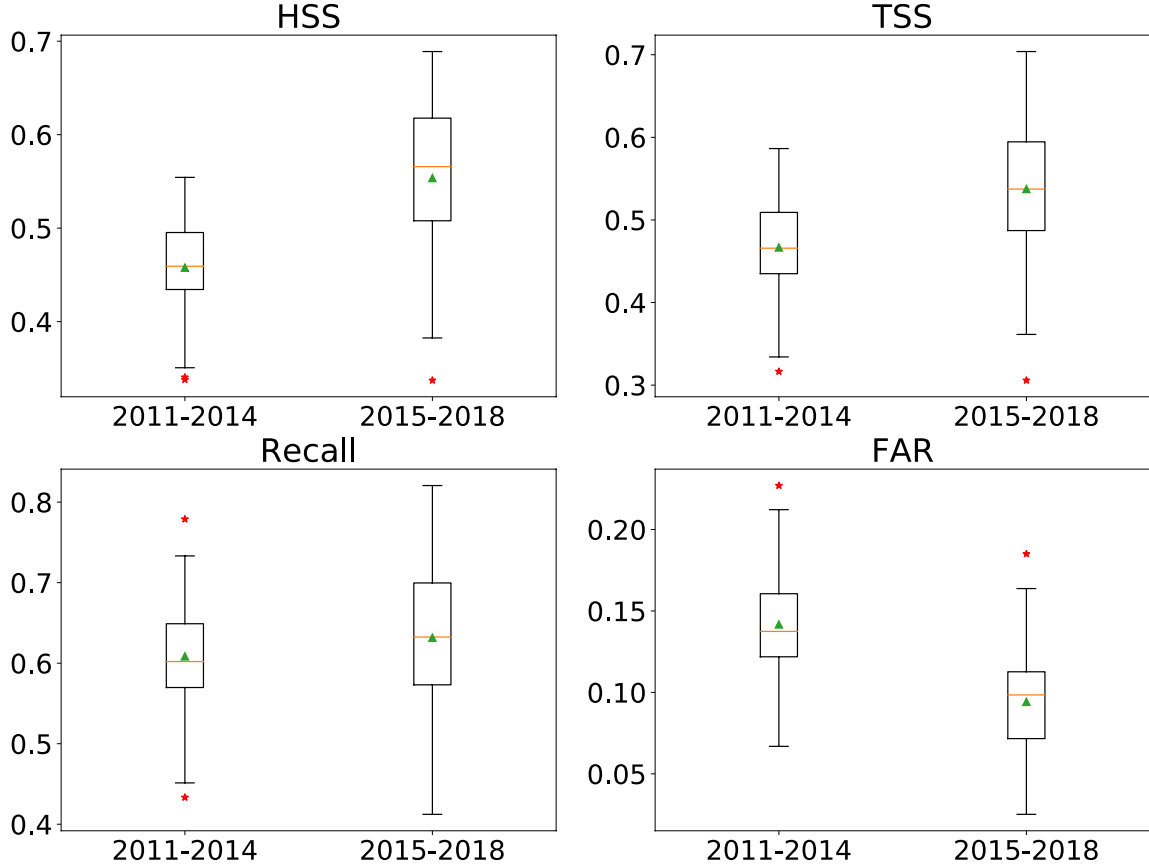


Figure 6. The boxplots of skill scores for predicting $\geq C$ flares. The training/testing are conducted within each group of years. The symbols in the figure are the same with previous boxplots.

6. CONCLUSION

In this paper, we built a dataset covering active regions from 2010 to 2018 from [Joint Science Operations Center \(jsoc.stanford.edu\)](http://jsoc.stanford.edu). Each data sample is the time sequence of 20 SHARP parameters which represent the magnetic field properties an active region. We developed a LSTM network to predict the maximum flare class Γ in next 24 hours of an active region. The prediction task is reduced to a binary classification task when Γ is larger than a certain threshold or not. We considered three different classes of Γ : $\geq M$, $\geq C$ and $\geq Q$ (Q refers to quiet). The training/testing splitting is done based on active regions which guarantees that the model does predictions on the data samples it has never seen previously. The skill scores produced by the model vary substantially for different years and we investigated the solar cycle dependence of the model performance. The main results of this paper are concluded as:

1. The LSTM based model achieves better performance of predicting solar flares than the previous approaches such as MLP, SVM, DeFN. The results are also comparable with the recently published work using LSTM method.
2. Although More than 50% percent of skill scores of LSTM model can be acquired from simple linear regression models, the non-linearity introduced by LSTM reduces the number of false alarms and improves the predictability of the model.
3. Previous works using active region data after 2015 for testing could introduce bias into the skill scores. If the model is trained on 2011-2014 and tested on 2015, it produces better skill scores than other combination of years. This relates to the difference of average level of solar activity in the training and testing sets. For predicting $\geq C$ flares, the model also gives better skill scores on the data after 2015.

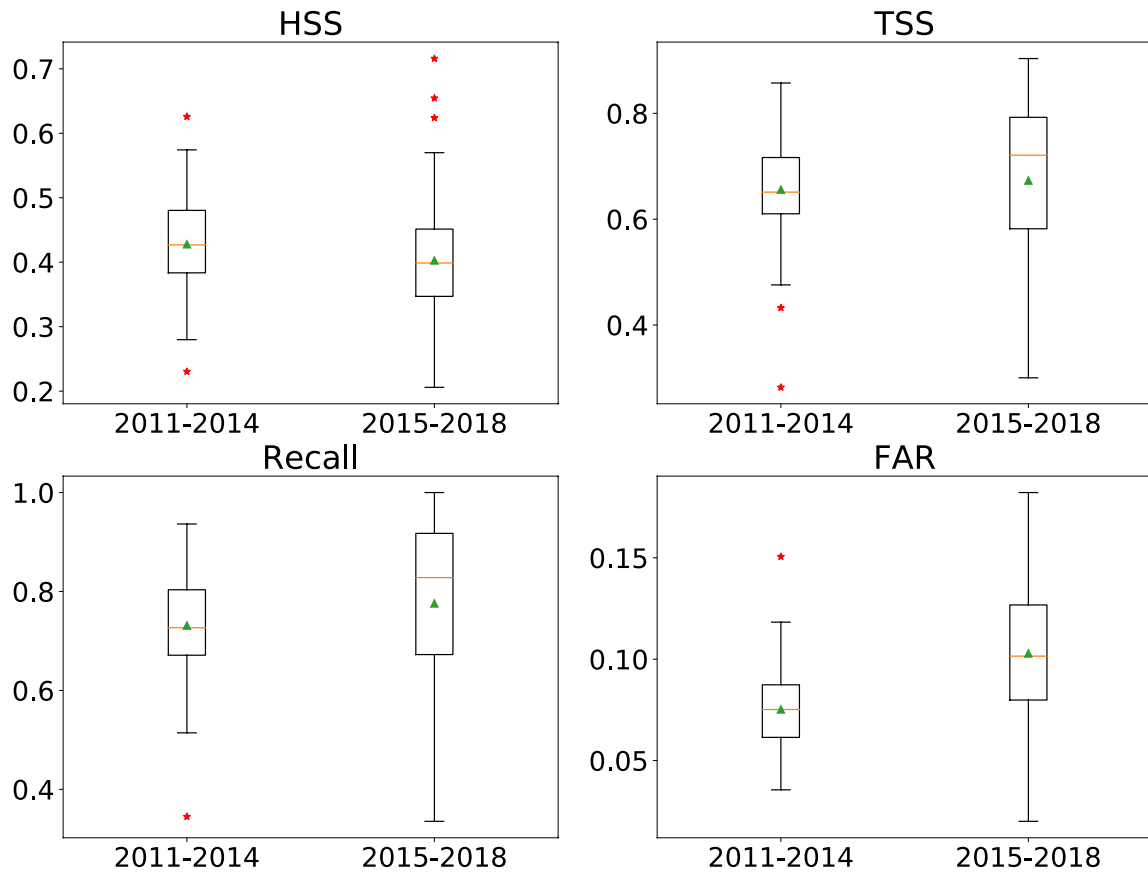


Figure 7. The boxplots of skill scores for predicting $\geq M$ flares. The training/testing are conducted within each group of years. The symbols in the figure are the same with previous boxplots.

Based on the results presented in this paper, LSTM is a valid method for solar flare prediction task. The skill scores from this paper are very close to those generated by another different LSTM model indicates that the information contained in the SHARP parameters is limited. In the future work, we plan to incorporate the image data from SDO mission into deep learning algorithms for solar flare prediction task.

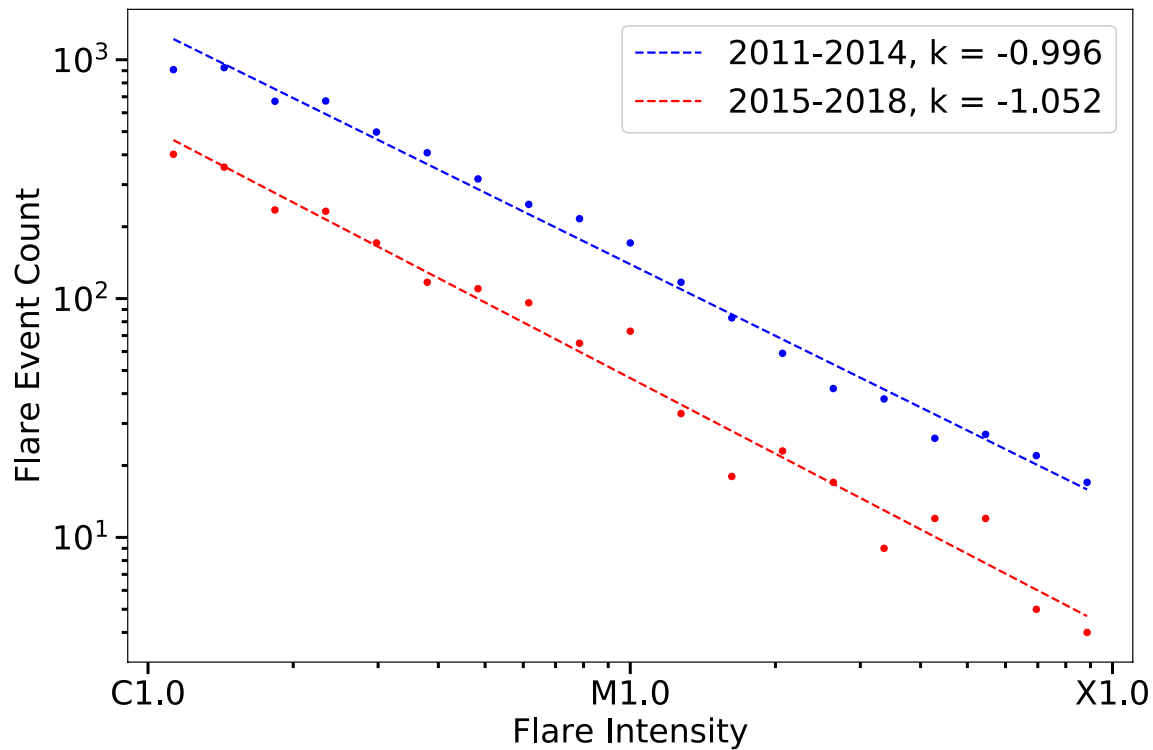


Figure 8. The histogram for C and M flares in two groups of years. The plot is in log-log scale and the histograms are straight lines which shows the intensity of flares agrees with the power-law distribution.

REFERENCES

- Ahmed, O. W., Qahwaji, R., Colak, T., et al. 2013, *SoPh*, 283, 157, doi: [10.1007/s11207-011-9896-1](https://doi.org/10.1007/s11207-011-9896-1)
- Barnes, G., Leka, K. D., Schrijver, C. J., et al. 2016, *ApJ*, 829, 89, doi: [10.3847/0004-637X/829/2/89](https://doi.org/10.3847/0004-637X/829/2/89)
- Bobra, M. G., & Couvidat, S. 2015, *ApJ*, 798, 135, doi: [10.1088/0004-637X/798/2/135](https://doi.org/10.1088/0004-637X/798/2/135)
- Bobra, M. G., Sun, X., Hoeksema, J. T., et al. 2014, *SoPh*, 289, 3549, doi: [10.1007/s11207-014-0529-3](https://doi.org/10.1007/s11207-014-0529-3)
- Boucheron, L. E., Al-Ghraibah, A., & McAteer, R. T. J. 2015, *ApJ*, 812, 51, doi: [10.1088/0004-637X/812/1/51](https://doi.org/10.1088/0004-637X/812/1/51)
- Florios, K., Kontogiannis, I., Park, S.-H., et al. 2018, *SoPh*, 293, 28, doi: [10.1007/s11207-018-1250-4](https://doi.org/10.1007/s11207-018-1250-4)
- Garcia, H. A. 1994, *SoPh*, 154, 275, doi: [10.1007/BF00681100](https://doi.org/10.1007/BF00681100)
- Gers, F. A., Schmidhuber, J., & Cummins, F. 1999
- Graves, A., Mohamed, A.-r., & Hinton, G. 2013, in 2013 IEEE international conference on acoustics, speech and signal processing, IEEE, 6645–6649
- Hastie, T., Tibshirani, R., Friedman, J., & Franklin, J. 2005, *The Mathematical Intelligencer*, 27, 83
- Hochreiter, S., & Schmidhuber, J. 1997, *Neural computation*, 9, 1735
- Hoeksema, J. T., Baldner, C. S., Bush, R. I., Schou, J., & Scherrer, P. H. 2018, *SoPh*, 293, 45, doi: [10.1007/s11207-018-1259-8](https://doi.org/10.1007/s11207-018-1259-8)
- Huang, X., Wang, H., Xu, L., et al. 2018, *ApJ*, 856, 7, doi: [10.3847/1538-4357/aaae00](https://doi.org/10.3847/1538-4357/aaae00)
- Jonas, E., Bobra, M., Shankar, V., Todd Hoeksema, J., & Recht, B. 2018, *SoPh*, 293, 48, doi: [10.1007/s11207-018-1258-9](https://doi.org/10.1007/s11207-018-1258-9)
- Liu, C., Deng, N., Wang, J. T. L., & Wang, H. 2017, *ApJ*, 843, 104, doi: [10.3847/1538-4357/aa789b](https://doi.org/10.3847/1538-4357/aa789b)
- Liu, H., Liu, C., Wang, J. T. L., & Wang, H. 2019, *ApJ*, 877, 121, doi: [10.3847/1538-4357/ab1b3c](https://doi.org/10.3847/1538-4357/ab1b3c)
- Muranushi, T., Shibayama, T., Muranushi, Y. H., et al. 2015, *Space Weather*, 13, 778, doi: [10.1002/2015SW001257](https://doi.org/10.1002/2015SW001257)
- Nishizuka, N., Sugiura, K., Kubo, Y., Den, M., & Ishii, M. 2018, *ApJ*, 858, 113, doi: [10.3847/1538-4357/aab9a7](https://doi.org/10.3847/1538-4357/aab9a7)

Qahwaji, R., & Colak, T. 2007, SoPh, 241, 195,
doi: [10.1007/s11207-006-0272-5](https://doi.org/10.1007/s11207-006-0272-5)

Song, H., Tan, C., Jing, J., et al. 2009, SoPh, 254, 101,
doi: [10.1007/s11207-008-9288-3](https://doi.org/10.1007/s11207-008-9288-3)

Yu, D., Huang, X., Wang, H., & Cui, Y. 2009, SoPh, 255,
91, doi: [10.1007/s11207-009-9318-9](https://doi.org/10.1007/s11207-009-9318-9)

Yuan, Y., Shih, F. Y., Jing, J., & Wang, H.-M. 2010,
Research in Astronomy and Astrophysics, 10, 785,
doi: [10.1088/1674-4527/10/8/008](https://doi.org/10.1088/1674-4527/10/8/008)